A Novel Air-to-Ground Channel Modeling Method Based on Graph Model

Wang, Nanxin; Yin, Xuefeng; Cai, Xuesong; Rodríguez-Piñeiro, José ; Pérez Yuste, Antonio ; Tian, Li

Published in:
13th European Conference on Antennas and Propagation (EuCAP)

Publication date:
2019

Document Version
Accepted author manuscript, peer reviewed version

A Novel Air-to-Ground Channel Modeling Method Based on Graph Model

Nanxin Wang[1], Xuefeng Yin[1], Xuesong Cai[2], José Rodríguez-Piñeiro[1], Antonio Pérez Yuste[3], and Li Tian[4]
[1]School of Electronics and Information Engineering, Tongji University, Shanghai, China
[2]Department of Electronic Systems, Aalborg University, Aalborg, Denmark
[3]School of Telecommunication Systems and Engineering, Technical University of Madrid, Spain
[4]ZTE Corporation, Shanghai, China
Email: [1]{1631501,yinxuefeng,j.rpineiro}@tongji.edu.cn, [2]xuc@es.aau.dk, [3]antonio.perez@upm.es and [4]tian.li150@zte.com.cn

***Abstract*—Air-to-ground (A2G) communication is envisioned to support numerous applications in 5G wireless networks. In this paper, an active measurement campaign for unmanned aerial vehicle (UAV) channels is introduced. Simulation based on Graph Model (GM) is also conducted for this specific measurement. Both the measured and simulated channel impulse responses (CIRs) are extracted. Based on the CIRs, the multipath components (MPCs) are estimated by using a high-resolution algorithm derived according to the space-alternating generalized expectation-maximization (SAGE) principle. The GM simulation performance is assessed by comparing the concatenated power delay profiles (CPDPs) and MPCs with the measurement results. In addition, an object-labeled clustering method is proposed to further analyze the low altitude UAV channel contributed by individual objects/buildings.**

***Index terms*—** Air-to-ground channel, graph model, clustering and building impacts.

I. Introduction

Unmanned aerial vehicles communication has been envisioned as an important technique in next generation wireless networks [1]. The mobility of UAVs allow supporting on demand communication, smart city monitoring, and data relaying applications [2]. Efforts have been taken to study the UAV channels based on both simulation methods [3] [4] and measurement methods [5] [6]. Basically, most simulation implementations are carried out by ray-tracing (RT) tools [7], which calculates the reflection paths by a image method, involving a large amount of calculation, especially for the high-order reflection links. Meanwhile, RT tools are usually used to simulate narrow-band characteristics in UAV channel.

The graph model, as a semi-deterministic radio channel modeling approach [8], is also expected to be suitable for UAV channel modeling to explore broadband characteristics. The GM was firstly proposed in [9], then the previous work was extended to the MIMO (multi-input multi-output) system, and a closed mathematical expression of the channel response was proposed in [10]. Subsequently, the graph model has been widely used in indoor scenarios [11], high-speed railway communication scenarios [12], and tunnel scenarios [13], etc.

This work was jointly supported by National Natural Science Foundation of China (NSFC) (Grant No. 61850410529 and No.61471268), the project "5G channel simulation and performance verification based on big data" under Grant No. 2018ZX03001031-003 of Ministry of Industry and Information Technology of People's Republic of China, and the project "Propagation channel measurements, parameter estimation and modeling for multiple scenarios" of Shanghai Institute of Microsystem and Information Technology, China Academy of Science. *Corresponding author: Xuefeng Yin.*

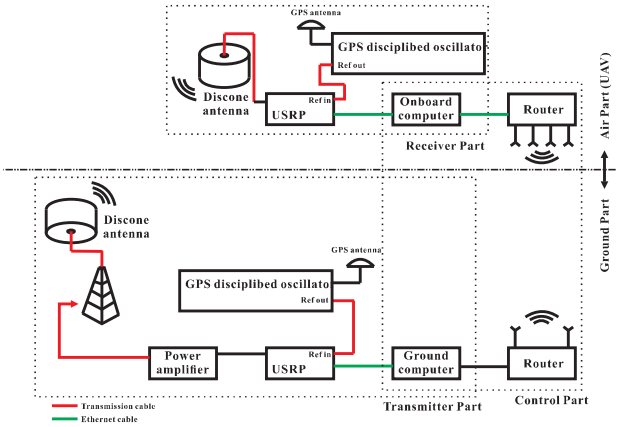

Fig. 1. Diagram of the equipment used during the measurement campaign.

For the purpose of further understanding the low altitude UAV A2G channel, the GM deviated in [8] is applied in this paper. The rest of this paper is organized as follows. Section II introduces the measurement campaign as well as the channel characterization. Section III describes the GM implementation procedures and shows the channel reconstruction results. To statistically analyze the environment interactions, a object-labeled clustering method is proposed in Section IV. A comparison for the object-labeled clusters is also conducted in Section IV. Finally conclusive remarks are addressed in Section V

II. UAV Channel Measurement and Characterization

In this section, the conducted measurement campaign is introduced including the equipment, scenario and experiment specifications. Furthermore, the CPDPs experienced by UAV are calculated, and based on the CPDPs, SAGE algorithm is used to estimate parameters of MPCs.

A. Measurement campaign

Fig. 1 illustrates a diagram of the equipment used during the UAV channel measurement. It consists of two

Fig. 2. Satellite view of the measurement scenario.

parts, i.e., the air part and the ground part. The air part was loaded on the UAV, which contains a quasi-omnidirectional packaged discone antenna, a Universal Software Radio Peripheral (USRP) device, a GPS-disciplined oscillator and a small computer. The ground part contains another set of equipments for signal transmitting. In addition, a pair of commercial wireless fidelity (WiFi) routers are used in both air part and ground part for remotely controlling.

The measurement was conducted in a suburban scenario at Jiading Campus, Tongji University, Shanghai. Fig. 2 illustrates the satellite view of the measurement scenario. The ground transmitting part was located at the white asterisk, where the antenna was mounted at $15\,\mathrm{m}$ by a height-variable tower. A horizontal round-trip flight was conducted with going height of $15\,\mathrm{m}$ and returning height of $25\,\mathrm{m}$. During the flight, the UAV flew across buildings and river with a speed of about $6\,\mathrm{m/s}$ and a total length of about 450m. The carrier frequency in the experiment was set to $850\,\mathrm{MHz}$ with bandwidth of $25\,\mathrm{MHz}$. The measurement began after the UAV reached 15 meters altitude and stopped before UAV landed.

B. Channel characterization

The CIRs from measurement are calculated as:

$$h(t,\tau) = \frac{\int r(t)s^*(t-\tau)\mathrm{d}t}{\int |s(t)|^2 \mathrm{d}t} \tag{1}$$

where $r(t)$ denotes the received signal, and $s(t)$ represents the transmitted pseudo noise sequence. By exploiting the CIR results, the SAGE algorithm is used to estimate parameters, i.e., delays, Doppler frequencies and complex amplitudes of MPCs. Readers can refer to [14] for details. The underlying signal model assumption for the SAGE algorithm in our case is formulated as

$$h(t,\tau) = \sum_{\ell=1}^{L(t)} \alpha_\ell(t)\delta(\tau-\tau_\ell(t))\exp\{j2\pi\int_0^t \nu_\ell(t)t\} + n(t,\tau) \tag{2}$$

The wave at t is characterized by its relative delay $\tau_\ell(t)$, Doppler frequency $\nu_\ell(t)$, and complex amplitude $\alpha_\ell(t)$. $L(t)$ is the total number of paths, $\ell \in [1,\ldots,L(t)]$ represents the index of multipath components, and $n(\tau,t)$ represents the white Gaussian noise.

The CPDPs and corresponding SAGE estimation results are illustrated in Fig. 3. It is noteworthy that the delays are relative values and the maximum power value is normalized to $0\,\mathrm{dB}$ for a more intuitive comparison with the GM simulated results. In Fig. 3(a), a dominant inverted V-shaped trajectory (contributed by LoS communication) can be observed, which is consistent with the going trip and returning trip. Meanwhile, a fuzzy positive V-shaped trajectory (very likely contributed by the building C) can also be found with the same central point. This positive V in returning part is clearer than it in going trip. This might be because of the flying height.

SAGE estimation results in delay domain and Doppler frequency domain are illustrated in Fig. 3(b) and Fig. 3(c), respectively. When observing the estimated Doppler frequency with relatively higher power, an S rotated by 90 degrees can be found. In this S curve, the Doppler frequency decreases from 0 to $-20\,\mathrm{Hz}$, then increases to $20\,\mathrm{Hz}$, and finally decreases again to $0\,\mathrm{Hz}$. This is because the UAV takes off near the ground transmitter where rich MPCs exist, then it leaves with stable speed at $20-60\,\mathrm{s}$, makes a U-turn flight at $60-100\,\mathrm{s}$ with a raise of $10\,\mathrm{m}$, and finally flies back at $100-160\,\mathrm{s}$.

III. UAV CHANNEL RECONSTRUCTION BASED ON GM

In this section, we exploit the graph simulation tool [8] to gain insights into UAV channel, including reconstructing the channel, channel estimation with SAGE algorithm. A object-labeled MPCs grouping method is proposed to further analyze the channel components contributed from individual objects/buildings.

A. GM implementation

In such a typical suburban scenario with buildings, river, grassland, road and trees, it is impractical to precisely model all the obstacles including their geometric locations, electromagnetic characteristics as well as surface roughnesses. Some simplifications are applied: i) grassland, river, and roads are modelled as a horizontal plane, ii) the building materials are considered the same, iii) trees and unimportant buildings are not involved. With the simplifications, the GM simulation is conducted as below:

- Set up a 3-D digital map. All the objects concluded are divided into multiple small tiles labeled with position and direction. The distance and angular between each pair of vertices are recorded.
- Set up the propagation graph. Evaluate the visibility for every pair of two nodes, and calculate the corresponding propagation coefficient.
- Calculate the channel transfer function by a frequency scan simulation (refer to [11]), the CIR is obtained by a inverse Fourier transform of the transfer function.

Fig. 4 illustrates the 3-D digital map applied in the GM implementation. The transmitter is noted as a black asterisk, the receiver loaded on UAV is marked as a set of red asterisks. Three main buildings (i.e., building A, building B and building C) as well as the ground are incorporated. In order to match the measurement scenario, the receiver

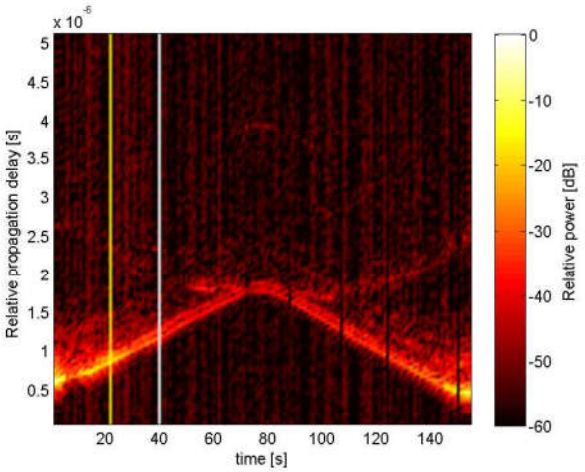

(a) Concatenated power delay profiles

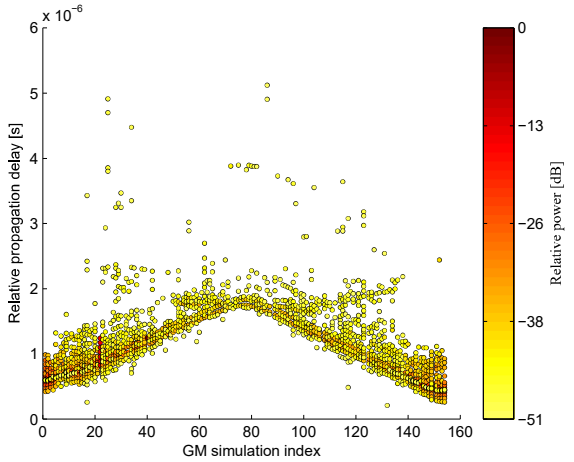

(b) SAGE estimation results in delay domain

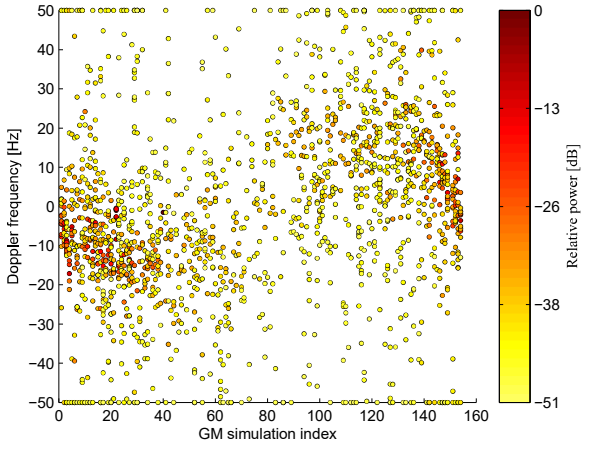

(c) SAGE estimation results in Doppler frequency domain

Fig. 3. CPDPs of measurement and corresponding SAGE estimation results in delay and Doppler domain.

is tied to a 3-D location and is time-stamped. That is, the receivers uniformly scattered in the UAV trajectory have a 6 m/s mobile relationship. However, the U-turn flight is not smoothly considered during the simulation, leading to a sudden change at the turning point.

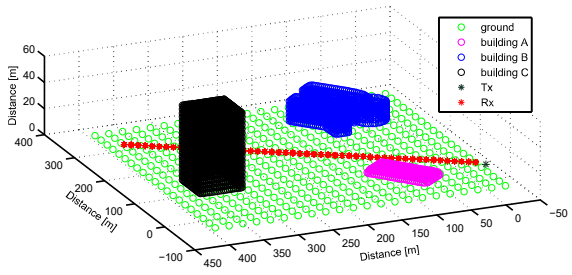

Fig. 4. Digital map established for this measurement scenario.

B. GM reconstructed results

The CPDPs reconstructed by the afore-mentioned GM procedures are illustrated in Fig. 5(a). Its SAGE estimation results in delay and Doppler frequency domain are shown in Fig. 5(b) and Fig. 5(c), respectively. By observing Fig. 5(a), we can find those two V-shaped trajectories are much more clear. A W-shaped trajectory, proved to be contributed by building B, is also visible. However, the components contributed by ground and building A are non-resolvable for LoS contribution due to the bandwidth limitation.

It can be observed from Fig. 5(c) that the SAGE estimated Doppler frequency from the reconstructed CPDPs is more regular. The dominant trajectory consists of two straight lines as we set a constant speed in GM. Roughly we can also find some other continuous curves, which are offered by objects in this scenario. These GM simulated results, seem similar to the measured results, shows the effectiveness of GM in simulating low altitude UAV channel.

IV. Object-labeled clustering based on GM

Cluster-based methods describing dispersion of propagation paths are adopted for constructing stochastic channel models [15]. Usually, multi-path clustering methods are implemented by iterative operations for minimizing the intra-cluster correlation and maximizing inter-cluster difference. Priori weights should be provided to each parameter. These clustering methods cannot identify which object has a directive impact on a certain cluster. However, GM is supported to record the propagation paths (for lower bounces), which means that it can identify the objects that promote each MPCs. We can redefine a clustering method as below: the MPCs in a cluster are contributed by the same object, MPCs in different clusters are contributed by different objects. According to this new definition, MPCs extracted from reconstructed CPDPs are grouped based on their different sources. For the purpose of comparison, the multi-path grouping is conducted again based on K-means clustering algorithm [16] for both measurement results and GM reconstructed results.

The clustering results are illustrated in Fig. 6. There are five adjacent snapshots involved in this measurement segmentation, and the UAV position in corresponding simulation segmentation is adjusted the same as it in real

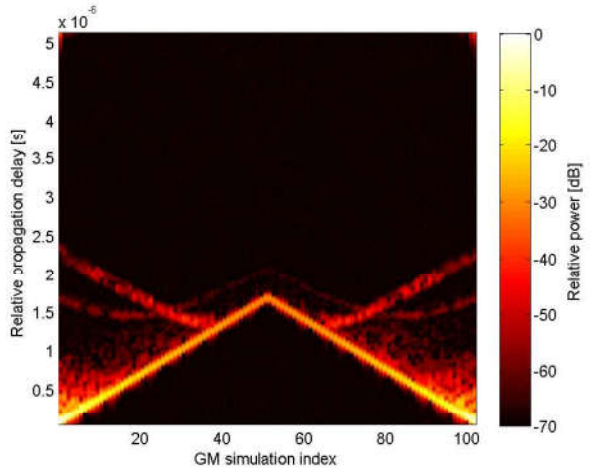

(a) Concatenated power delay profiles

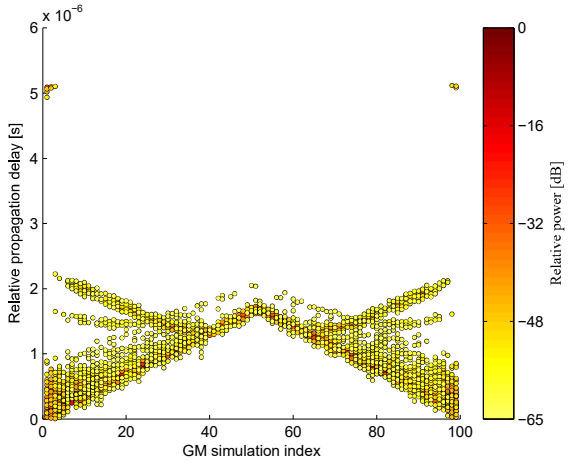

(b) SAGE estimation results in delay domain

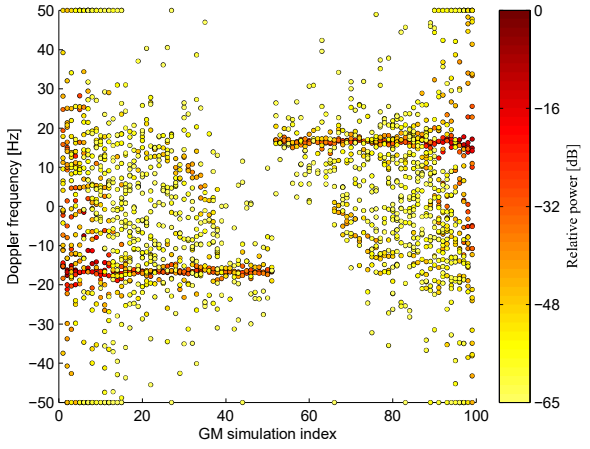

(c) SAGE estimation results in Doppler frequency domain

Fig. 5. GM reconstructed CPDPs and its SAGE estimation results in delay and Doppler domain.

measurement. During a segmentation, the UAV channel is observed to be slightly changed. Clustering results based on K-means algorithm for MPCs extracted from both measured and simulated data are shown in Fig. 6(a) and Fig. 6(b), respectively. We can find that the grouping here is mainly conducted by delay differences. Fig. 6(c) (same components as Fig. 6(b)) illustrates the object-labeled grouping results. We can also find that the cluster contributed by ground and LoS is mixed with the cluster contributed by building A. Building B and C offer similar delays but different Doppler frequencies, which is not easy to be recognized by K-means algorithm.

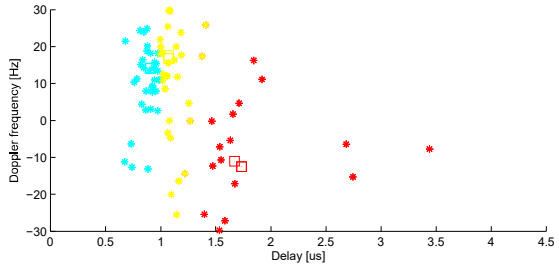

(a)

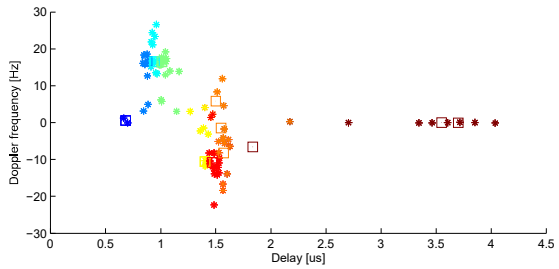

(b)

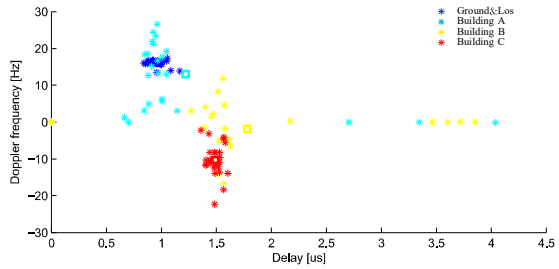

(c)

Fig. 6. Multi-path grouping for SAGE estimation results in delay and Doppler domain. (a) K-means grouping results for MPCs extracted from measurement data. (b) K-means grouping results for MPCs extracted from GM simulated data. (c) Object-labeled grouping results for MPCs extracted from GM simulated data.

Buildings have different impacts on MPCs, including mean delay, mean Doppler frequency, delay spread and Doppler frequency spread. Fig. 7 shows the individual impacts from four object-labeled clusters and from the complete environment. The horizontal axe, the segmentation index, also represents the flying trajectory. A sliding window is used during segmenting, to guarantee its precision. We can find that the power is mainly contributed by the ground&LoS part. The power varies along the whole flight with path loss, shadowing and building impacts. Convincingly, the power contributed by building C meets a deep shadowing among segmentation index $40-60$. The delay contributions illustrated in Fig. 7(b) are related to their relative position with UAV. Fig. 7(c) shows that the root mean square (RMS) delay spreads, contributed by

Table I. $\bar{\tau}$, τ_{rms}, $\bar{\nu}$, ν_{rms} for object-labeled clusters

Objectes	$\bar{\tau}$ [ns]	τ_{rms} [ns]	$\bar{\nu}$ [Hz]	ν_{rms} [Hz]
Total	210.7	218.5	14.98	2.27
Ground&Los	204.1	210.4	15.36	1.47
Building A	362.6	82.5	8.93	4.65
Building B	1554.5	119.9	6.54	5.66
Building C	1523.0	194.9	9.11	5.42

each object, jitter a lot along the trajectory. Roughly we can find that the RMS delay spread decreases with the distance between UAV and ground transmitter.

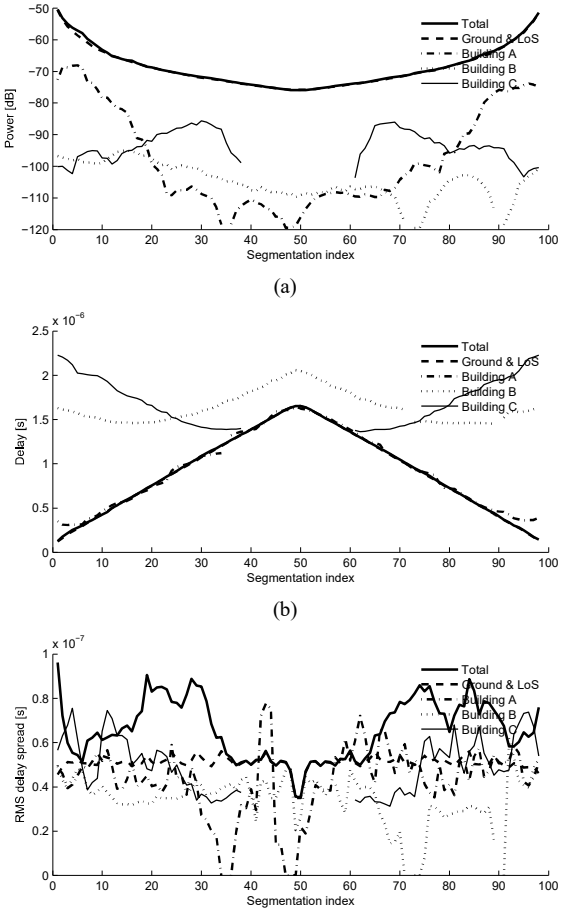

Fig. 7. Object-labeled clusters impacts on UAV channel. (a) Power. (a) Delay. (a) RMS delay spread.

Tab. I illustrates the mean delay, RMS delay spread, mean Doppler frequency, and RMS Doppler frequency spread for the object-labeled clusters in the whole flight. The total parameters is mainly effected by Ground&Los components, which provide a large RMS delay spread and a small RMS Doppler frequency spread. Meanwhile, the buildings provide relative smaller RMS delay spread but larger RMS Doppler frequency spread. These intra or inter cluster parameters are essential to gain insight into how the environment interacts with the communication channel.

V. Conclusions

In this contribution, an active UAV channel measurement is conducted. SAGE algorithm is applied to estimating multipath components and further analyzing the concatenated power delay profiles. For the purpose of study environmental interactions to low altitude UAV channel, propagation graph simulation tool is exploited to reconstruct the CPDPs of this scenario. Results prove its effectiveness in simulating CPDPs and MPCs in UAV channel. In addition, the object-labeled clustering method is proposed for a prior study of individual object impacts on wireless communication channel. More works based on GM will be investigated to enrich the novel channel modeling method, and further figure out how the environment interacts with the low altitude UAV channel.

References

[1] Y. Zeng, R. Zhang, and J. L. Teng, "Wireless communications with unmanned aerial vehicles: opportunities and challenges," *IEEE Communications Magazine*, vol. 54, no. 5, pp. 36–42, 2016.

[2] A. S. I. Nadisanka Rupasinghe and I. Guvenc, "Optimum hovering locations with angular domain user separation for cooperative uav networks," in *Global Communications Conference*, 2016, pp. 1–6.

[3] Q. Feng, J. Mcgeehan, E. K. Tameh, and A. R. Nix, "Path loss models for air-to-ground radio channels in urban environments," in *Vehicular Technology Conference, 2006. Vtc 2006-Spring. IEEE*, 2006, pp. 2901–2905.

[4] W. Khawaja, O. Ozdemir, and I. Guvenc, "UAV air-to-ground channel characterization for mmwave systems," 2017.

[5] D. W. Matolak, "Channel characterization for unmanned aircraft systems," in *Military Communications Conference, Milcom*, 2015, pp. 1656–1660.

[6] W. Khawaja, I. Guvenc, and D. Matolak, "UWB channel sounding and modeling for uav air-to-ground propagation channels," in *Global Communications Conference*, 2017, pp. 1–7.

[7] J. W. Mckown and R. L. Hamilton, "Ray tracing as a design tool for radio networks," *IEEE Network*, vol. 5, no. 6, pp. 27–30, 1991.

[8] L. Tian, V. Degli-Esposti, E. M. Vitucci, and X. Yin, "Semi-deterministic radio channel modeling based on graph theory and ray-tracing," *IEEE Transactions on Antennas & Propagation*, vol. 64, no. 6, pp. 2475–2486, 2016.

[9] T. Pedersen and B. H. Fleury, "A realistic radio channel model based in stochastic propagation graphs," 2006.

[10] ——, "Radio channel modelling using stochastic propagation graphs," in *IEEE International Conference on Communications*, 2007, pp. 2733–2738.

[11] T. Pedersen, G. Steinbock, and B. H. Fleury, "Modeling of reverberant radio channels using propagation graphs," *IEEE Transactions on Antennas & Propagation*, vol. 60, no. 12, pp. 5978–5988, 2012.

[12] L. Tian, X. Yin, Q. Zuo, and J. Zhou, "Channel modeling based on random propagation graphs for high speed railway scenarios," in *IEEE International Symposium on Personal, Indoor and Mobile Radio Communications*, 2012, pp. 1746–1750.

[13] J. Zhang, C. Tao, L. Liu, and R. Sun, "A study on channel modeling in tunnel scenario based on propagation-graph theory," in *Vehicular Technology Conference*, 2016, pp. 1–5.

[14] B. H. Fleury, M. Tschudin, R. Heddergott, and D. Dahlhaus, "Channel parameter estimation in mobile radio environments using the sage algorithm," *Selected Areas in Communications IEEE Journal on*, vol. 17, no. 3, pp. 434–450, 1999.

[15] M. Steinbauer, A. F. Molisch, and E. Bonek, "The double-directional radio channel," *IEEE Antennas & Propagation Magazine*, vol. 43, no. 4, pp. 51–63, 2001.

[16] N. Czink, P. Cera, J. Salo, and E. Bonek, "Improving clustering performance using multipath component distance," *Electronics Letters*, vol. 42, no. 1, pp. 33–5, 2006.